Multiple-qubit controlled unitary quantum gate for Rydberg atoms using shortcut to adiabaticity and optimized geometric quantum operations

Meng Li,[1] F.-Q. Guo,[1] Z. Jin,[2] L.-L. Yan,[1,*] E.-J. Liang,[1,†] and S.-L. Su[1,‡]

[1]*School of Physics, Key Laboratory of Materials Physics of Ministry of Education, Zhengzhou University, Zhengzhou 450001, China*

[2]*School of Physics, Northeast University, Shenyang 110819, China*

(Received 8 March 2021; accepted 26 May 2021; published 15 June 2021)

Multiple-qubit quantum logic gates are an important element in the implementation of quantum computers. The direct construction of multiple-qubit quantum logic gates in an efficient way has important values compared to the construction of multiple-qubit gates using a series of two-qubit and single-qubit gates. We propose a scheme to construct a multiple-qubit C_kU gate (k denotes the number of control qubits and U means the arbitrary universal operation performed on the target qubit) in a neutral atom platform through the Rydberg blockade effect by successively exciting them to Rydberg states. This scheme takes advantage of the shortcut to adiabaticity of inverse engineering, geometric quantum operations, as well as optimized control theory. The geometric quantum computation considered in this manuscript guarantees the robustness to operational errors. Meanwhile, inverse engineering-based shortcut to adiabaticity provides a further advantage in terms of the speed of the system evolution compared to adiabatic processes. An additional feature of our multiple-qubit quantum logic gate is that arbitrary operation on the target atom can be realized by adjusting the amplitude and phase of the laser fields. Numerical simulation of the master equation based on the full Hamiltonian demonstrates the high fidelity of the proposed scheme and its robustness to operational errors and spontaneous emission.

DOI: 10.1103/PhysRevA.103.062607

I. INTRODUCTION

Rydberg atoms, by exciting the neutral atoms into the high principal quantum number state, have provided a promising platform in the past decade for the processing of quantum information due to their various excellent properties, e.g., strong and long-range interaction, long lifetime, and giant polarizability [1–7]. The strong interaction between Rydberg atoms induces the Rydberg blockade effect [8–13], which can be applied to construct fast, high-fidelity, and stable quantum logic gates [14–23]. Recent experimental developments have demonstrated the great potential of Rydberg atoms in quantum information processing [24–29].

Geometric quantum computation (GQC) has strong resistance to local interference since the Abelian or non-Abelian geometric phase of the quantum state is dependent only on the cyclic evolution for the path of the Hilbert space [30–34]. In previous studies, GQC has often been used for the adiabatic evolution accompanied by a long duration and results in a great decoherence [35–37]. In order to overcome this defect, it is applied to nonadiabatic evolution to build a nonadiabatic holonomic quantum computation (NHQC) based on the non-Abelian geometric phases [38,39]. After that, various theoretical and experimental schemes via NHQC emerge one after another [40–52]. However, there are still many strict restrictions on the Hamiltonian. In recent years, many efforts have been carried out to expand NHQC by utilizing different methods, such as the dynamic decoupling (DD) [53,54], single-shot-shaped (SSSP) [49,55–58], and single loop [59–62] methods. Furthermore, combining with different quantum systems is also an important research direction, for example, superconducting [63–65], NV-center [66], and nuclear magnetic resonance (NMR) [67,68] systems.

Stimulated Raman adiabatic passage is insensitive to the fluctuation of parameters [69–72], such as the shape, intensity, and frequency of the laser pulse, and requires long evolution time, which would enhance the influence of decoherence. To address this issue, shortcut to adiabaticity (STA) is proposed and has attracted much attention in recent years [73–81], which keeps the advantage of the adiabatic method but with a shortened evolution time. A variety of methods has been found to implement STA in past studies, such as transitionless quantum driving [82,83], Lewis-Riesenfeld (LR) invariant-based inverse engineering method [84–91], and digitized adiabatic quantum computing [92].

Multiple-qubit quantum logic gates as the foundation of quantum computation have been constructed in the past few decades by using different methods through combining the several single- and two-qubit logic gates [72,93–97]. However, with an increasing number of qubits, the required number of single- and two-qubit gates will increase exponentially [97]. The straightforward construction of a multiple-qubit logic gate greatly reduces the difficulty of gate operation and shortens the operation time since the number of operations grows polynomially with the increase of qubits, which can save the quantum resources effectively. The Rydberg atoms are ideal candidates for the development of straightforward multiple-qubit gates due to their special properties [29,98–102].

*llyan@zzu.edu.cn
†ejliang@zzu.edu.cn
‡slsu@zzu.edu.cn

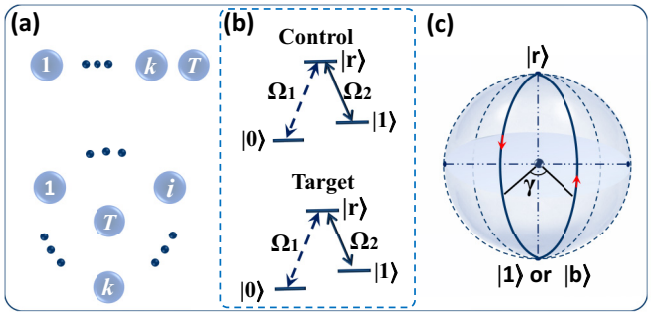

FIG. 1. (a) One-dimensional and two-dimensional configuration for realizing a multiple-qubit C_kU gate (k represents the number of control atoms and T represents the target atom). (b) Energy level of the control and target qubits for the C_kPG gate ($\Omega_1 = 0$, $\Omega_2 = \Omega_0$; the case in Sec. II A) and C_kU gate (the case in Secs. II B and II C). The qubit consists of the ground states $|0\rangle$ and $|1\rangle$, and $|r\rangle$ denotes the Rydberg state of atoms with the parameters. $\Omega_{0,1,2}$ denotes the Rabi frequency of the lasers. Every two atoms have the strength V_{ij} of Rydberg-Rydberg interaction with each other. Due to the Rydberg blockade effect, only one atom can be excited to the Rydberg state $|r\rangle$. (c) Geometric illustration of the gate with a cyclic evolution for the orange-slice-shaped path on a Bloch sphere, where the bright state $|b\rangle$ is the superposition state of $|0\rangle$ and $|1\rangle$.

In this manuscript, we use shortcut to adiabaticity, geometric quantum operations, as well as optimized control theory to construct the fast and robust multiple-qubit C_kU quantum logic gate in the Rydberg atomic system. In contrast to the existing theoretical and experimental schemes, the present one has the following characteristics: (i) The influence of the decay is reduced in contrast to the stimulated Raman adiabatic passage by taking advantage of the shortcut to adiabaticity method and the influence of the operational error is minimized through the geometric quantum operation, which has inherent noise resistance to parameter fluctuation. (ii) The scheme is compatible with the optimal control method, which can be used for obtaining higher fidelity and robustness. (iii) The desired C_kU can realize arbitrary single-qubit operation U on the target qubit conditioned on the k control qubits by modulating the laser parameters, which includes not only C_kNOT and C_kPhase gates (C_kPG), but also more general gates that have extensive application in quantum circuit and quantum Fourier transformation [97].

The article is organized as follows. In Sec. II, fast and robust multiple-qubit C_kU gates are constructed based on the shortcut to adiabaticity and optimized geometric quantum operation in a Rydberg atoms system; then we evaluate the performance of the gate. In Sec. III, we discuss some aspects of the experimental considerations, including the realization of pulse, actual Rydberg atomic level structure, and error analysis. Section IV is for the discussion and conclusion.

II. MODEL AND REALIZATION OF THE GATES

As shown in Fig. 1, the quantum gate consists of N atoms including k control qubits and one target qubit in our scheme. Each atom consists of two ground states $|0\rangle$, $|1\rangle$ and one Rydberg state $|r\rangle$. The interaction Hamiltonian between the Rydberg states is $H_I = \sum_{i<j}^{N} V_{i,j}\,\sigma_i^{rr} \otimes \sigma_j^{rr}$, where $V_{i,j}$ denotes the Rydberg-Rydberg interaction between the ith and jth atoms with the strength $V_{i,j} \gg \Omega_0$ and the operators $\sigma_m^{rr} = |r\rangle_m\langle r|$ $(m = i, j)$. Without loss of generality, in the following we suppose $V_{i,j} = V$ for the sake of analysis. When the laser pulse excites the ground state $|1\rangle$ of one atom to the Rydberg state, other qubits can no longer be excited to the $|r\rangle$ state due to the Rydberg blockade effect [1–3]. In the following, we will introduce our multiple-qubit quantum gate by considering the target qubit in a different coupling configuration.

A. The C_2PG gate

For simplicity, we consider a three-atom situation in our scheme, where the Hamiltonian of the control and target atoms can be rewritten as ($\hbar = 1$)

$$H_0 = \Omega_0 e^{i\Phi_0}|1\rangle_m\langle r| + \text{H.c.}\ (m = 1, 2, T). \tag{1}$$

The evolution of the system under the Hamiltonian H_0 is governed by the Schrödinger equation

$$i\frac{\partial}{\partial t}|\Psi_{(t)}\rangle = H_0(t)|\Psi_{(t)}\rangle. \tag{2}$$

In the computation subspace of $|1\rangle$ and $|r\rangle$, the state $|\Psi_{(t)}\rangle$ can be parameterized as

$$|\Psi_{(t)}\rangle = e^{-ig}\begin{pmatrix}\cos\frac{\chi}{2}e^{-i\varphi/2}\\ \sin\frac{\chi}{2}e^{i\varphi/2}\end{pmatrix}. \tag{3}$$

Inserting $|\Psi_{(t)}\rangle$ into Eq. (2), we can obtain the following equations:

$$\begin{aligned}\dot{g} &= -\dot{\varphi}/(2\cos\chi),\\ \dot{\chi} &= -2\Omega_0\sin(\Phi_0+\varphi),\\ \dot{\varphi} &= -2\Omega_0\cot\chi\cos(\Phi_0+\varphi).\end{aligned} \tag{4}$$

In order to make the initial state of the system cyclically evolved along the projection subspace under the drive of the H_0, a set of suitable parameters φ and χ can be selected to obtain Φ_0 and Ω_0 according to the conditions of Eq. (4), i.e.,

$$\Phi_0 = \arctan\left(\frac{\dot{\chi}}{\dot{\varphi}}\cot\chi\right) - \varphi, \quad \Omega_0 = -\frac{\dot{\chi}}{2\sin(\Phi_0+\varphi)}. \tag{5}$$

If the parameters satisfy the above equations, a pure geometric phase will be obtained after the cyclic evolution. The specific operation steps are described as follows.

Step (i): In order to achieve the goal of cyclic evolution, the boundary condition should be satisfied first,

$$\chi(0) = \chi(t_f) = 0. \tag{6}$$

Subsequently, we choose a set of parameters to make the initial state evolve from $|1\rangle$ to itself, and produce a phase factor which includes the dynamic phase and the geometric phase, where the dynamic phase is $\gamma_d(t_1, t_2) = -\int_{t_1}^{t_2}\langle\Psi_{(t)}|H_0|\Psi_{(t)}\rangle dt$, and the geometric phase is $\gamma_g(t_1, t_2) = i\int_{t_1}^{t_2}\langle\widetilde{\Psi}_{(t)}|\frac{d}{dt}|\widetilde{\Psi}_{(t)}\rangle dt$ [30,34] with $|\widetilde{\Psi}_{(t)}\rangle = e^{ig}|\Psi_{(t)}\rangle$. In order to get a pure geometric phase, we select the appropriate χ and φ to make the overall dynamic phase equal to zero in

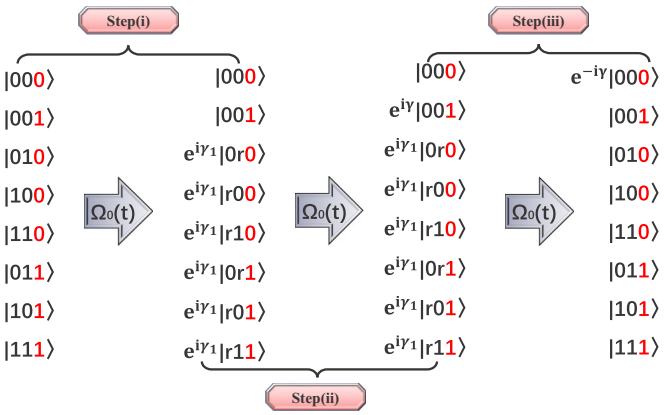

FIG. 2. The evolution steps of the C_2PG gate contain two control atoms (black) and one target atom (red). It should be noted that step (i) means the sequential driving on the control atoms one by one. In other words, step (i) actually consists of k (here, $k = 2$) small steps. And only the first atom in the $|1\rangle$ state can be excited to a Rydberg state. Step (ii) is the operation to achieve the geometric phase operation on the target atom. Step (iii) is the reverse operation of step (i).

steps (i)–(iii). In step (i), the laser should successively couple with the control atoms one by one. Step (i) can be divided into two small steps for the C_2PG gate. In the first small step $t \in (0, \frac{t_f}{2}]$, we illuminate the control atom 1 with the laser pulse determined by

$$\chi_{1,c1} = \pi \sin^2\left(\frac{\pi t}{t_f}\right), \quad \varphi_{1,c1} = -\frac{\pi}{4}\sin\left(\frac{2\pi t}{t_f}\right). \tag{7}$$

The corresponding evolution operator is obtained as $U_{1,c1} = e^{i\gamma_1}|r\rangle_1\langle 1| + e^{-i\gamma_1}|1\rangle_1\langle r| + |0\rangle_1\langle 0|$, where $\gamma_1 = \gamma_d(0, \frac{t_f}{2}) + \gamma_g(0, \frac{t_f}{2})$ denotes the achieved phase on the control atom 1 after this small step. In the second small step $t \in (\frac{t_f}{2}, t_f]$, we use the same pulse parameters,

$$\chi_{1,c2} = \pi \sin^2\left[\frac{\pi\left(t - \frac{t_f}{2}\right)}{t_f}\right],$$
$$\varphi_{1,c2} = -\frac{\pi}{4}\sin\left[\frac{2\pi\left(t - \frac{t_f}{2}\right)}{t_f}\right], \tag{8}$$

to couple control atom 2, and the same operator, i.e., $U_{1,c2} = e^{i\gamma_1}|r\rangle_2\langle 1| + e^{-i\gamma_1}|1\rangle_2\langle r| + |0\rangle_2\langle 0|$, would be achieved on atom 2 if atom 1 is not excited, where $\gamma_1 = \gamma_d(\frac{t_f}{2}, t_f) + \gamma_g(\frac{t_f}{2}, t_f) = \gamma_d(0, \frac{t_f}{2}) + \gamma_g(0, \frac{t_f}{2})$ denotes the achieved phase on control atom 2 after this small step. Otherwise, the operation on control atom 2 would be blocked due to the Rydberg-Rydberg interaction. That is, at most, only one control atom can obtain the transformations $|1\rangle \to e^{i\gamma_1}|r\rangle$ [see Fig. 2, step (i)].

Step (ii): The laser is turned on to illuminate the target atom to couple $|1\rangle$ with $|r\rangle$ in the time $t \in (t_f, 2t_f]$, with the parameters

$$\chi_t = \pi \sin^2\left[\frac{\pi(t - t_f)}{t_f}\right], \quad t \in (t_f, 2t_f],$$
$$\varphi_t = \begin{cases} -\frac{\pi}{4}\sin\left[\frac{2\pi(t-t_f)}{t_f}\right], & t \in \left(t_f, \frac{3t_f}{2}\right] \\ \frac{\pi}{4}\sin\left[\frac{2\pi(t-t_f)}{t_f}\right] - \gamma, & t \in \left(\frac{3t_f}{2}, 2t_f\right], \end{cases} \tag{9}$$

where γ can be an arbitrary angle. If any of the control atoms is not excited to a Rydberg state, the evolution operator in step (ii) can be obtained as $U_{2,T} = e^{i\gamma}|1\rangle_T\langle 1| + e^{-i\gamma}|r\rangle_T\langle r| + |0\rangle_T\langle 0|$ [103]. Otherwise, the evolution of the target atom would be blocked [see step (ii) in Fig. 2].

Step (iii): This step is the reverse of step (i). Concretely, in this step, the parameters for the pulse coupled with atom 2 for $t \in (2t_f, \frac{5t_f}{2}]$ are set as

$$\chi_{2,c2} = \pi \sin^2\left[\frac{\pi\left(t - \frac{3t_f}{2}\right)}{t_f}\right],$$
$$\varphi_{2,c2} = \frac{\pi}{4}\sin\left[\frac{2\pi\left(t - \frac{3t_f}{2}\right)}{t_f}\right] - \gamma'. \tag{10}$$

The parameters for the pulse coupled with control atom 1 for $t \in (\frac{5t_f}{2}, 3t_f]$ are set as

$$\chi_{2,c1} = \pi \sin^2\left[\frac{\pi(t - 2t_f)}{t_f}\right],$$
$$\varphi_{2,c1} = \frac{\pi}{4}\sin\left[\frac{2\pi(t - 2t_f)}{t_f}\right] - \gamma'. \tag{11}$$

Then, in step (iii), the evolution operator for control atoms 1 and 2 are, respectively, $U_{3,c1} = e^{i\gamma_3}|1\rangle_1\langle r| + e^{-i\gamma_3}|r\rangle_1\langle 1| + |0\rangle_1\langle 0|$, $U_{3,c2} = e^{i\gamma_3}|1\rangle_2\langle r| + e^{-i\gamma_3}|r\rangle_2\langle 1| + |0\rangle_2\langle 0|$, where $\gamma_3 = \gamma_d(2t_f, \frac{5t_f}{2}) + \gamma_g(2t_f, \frac{5t_f}{2}) = \gamma_d(\frac{5t_f}{2}, 3t_f) + \gamma_g(\frac{5t_f}{2}, 3t_f)$ denotes the achieved phase on control atoms 2 and 1, respectively, in step (iii). Combining steps (i) with (iii), the evolution operator for control atoms 1 and 2 is $U_{c1} = e^{i(\gamma_1+\gamma_3)}|1\rangle_1\langle 1| + e^{-i(\gamma_1+\gamma_3)}|r\rangle_1\langle r| + |0\rangle_1\langle 0|$ and $U_{c2} = e^{i(\gamma_1+\gamma_3)}|1\rangle_2\langle 1| + e^{-i(\gamma_1+\gamma_3)}|r\rangle_2\langle r| + |0\rangle_2\langle 0|$. One can get $\gamma_1 + \gamma_3 = \gamma'$, and set $\gamma' = \gamma$.

After the above three steps, we can obtain the multiple-qubit quantum controlled phase gate $e^{i\gamma}(|001\rangle\langle 001| + |010\rangle\langle 010| + |100\rangle\langle 100| + |110\rangle\langle 110| + |011\rangle\langle 011| + |101\rangle\langle 101| + |111\rangle\langle 111|) + |000\rangle\langle 000|$, which is equivalent to realizing an arbitrarily geometric phase gate $e^{-i\gamma}|000\rangle\langle 000| + |001\rangle\langle 001| + |010\rangle\langle 010| + |100\rangle\langle 100| + |110\rangle\langle 110| + |011\rangle\langle 011| + |101\rangle\langle 101| + |111\rangle\langle 111|$ [see step (iii) in Fig. 2].

B. The C_2U gate

As shown in Fig. 1(b), the Hamiltonian of the control and target atoms is obtained as

$$H = \tfrac{1}{2}(\Omega_1 e^{i\Phi_1}|0\rangle_m + \sqrt{2}\Omega_2 e^{-i\Phi_2}|1\rangle_m)\langle r| + \text{H.c.} \tag{12}$$

Setting $m = 1, 2, T$ and $\Omega = \sqrt{\Omega_1^2 + 2\Omega_2^2}/2$, we can obtain the bright state $|b\rangle = \sin\alpha|0\rangle - \cos\alpha e^{-i\Phi}|1\rangle$ and the decoupled dark state $|d\rangle = -\sin\alpha|1\rangle - \cos\alpha e^{i\Phi}|0\rangle$, where $\Phi = \Phi_1 + \Phi_2 + \pi$ and $\tan\alpha = \Omega_1/(\sqrt{2}\Omega_2)$. It should be noted that although Ω_1 and Ω_2 are time dependent, $\alpha = \arctan[\Omega_1/(\sqrt{2}\Omega_2)]$ could be a constant when the ratio between Ω_1 and Ω_2 is invariant. Meanwhile, although Φ_1 and Φ_2 are time dependent, the parameter Φ can be time independent when $\Phi_1 + \Phi_2$ is a constant. After setting α and Φ as time-independent parameters, $|b\rangle$ and $|d\rangle$ are time independent. On

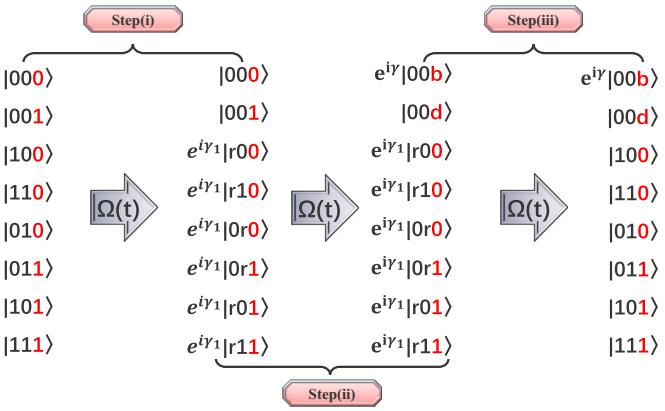

FIG. 3. The diagram shows the evolution steps of the C_kU ($k = 2$) gate containing two control atoms (black) and one target atom (red), where $|b\rangle$ is the superposition state of $|0\rangle_T$ and $|1\rangle_T$. Step (i) means the sequential driving on control atoms one by one, i.e., step (i) actually consists of k ($k = 2$) small steps. And only the first atom in the $|1\rangle$ state can be excited to Rydberg state $|r\rangle$. Step (ii) is the operation to achieve the geometric phase operation on the target atom. Step (iii) is the reverse operation of step (i).

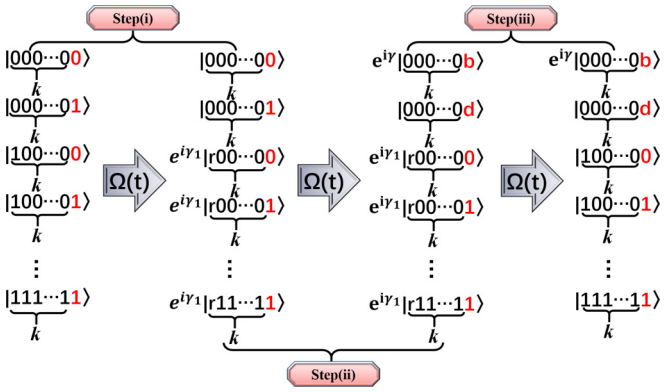

FIG. 4. The diagram shows the evolution steps of the C_kU gate containing k control atoms (black) and one target atom (red), where $|b\rangle$ is the superposition state of $|0\rangle_T$ and $|1\rangle_T$. Step (i) means the sequential driving on control atoms one by one, i.e., step (i) actually consists of k small steps. And only the first atom in the $|1\rangle$ state can be excited to Rydberg state $|r\rangle$. Step (ii) is the operation to achieve the geometric phase operation on the target atom. Step (iii) is the reverse operation of step (i).

that basis, Eq. (12) can be simplified to

$$H = \Omega e^{i\Phi_1}|b\rangle_m\langle r| + \text{H.c.}\ (m = 1, 2, T). \tag{13}$$

Similar to Eq. (1), the parameters in Hamiltonian (13) should also satisfy certain relation and boundary conditions similar to that in Eqs. (4)–(6). However, the involved bases are $|b\rangle$, $|r\rangle$, and $|d\rangle$ ($|d\rangle$ is time independent and does not evolve). That is, if the parameters in Eq. (13) are set the same as in Eq. (1), the evolution operator for $|b\rangle$, $|r\rangle$, and $|d\rangle$ in this section is similar to that for $|1\rangle$, $|r\rangle$, and $|0\rangle$ in Sec. II A. Here we also divide the execution for the C_kU ($k = 2$) gate into three steps.

Step (i): Similarly to step (i) in Sec. II A, in this step we can get the evolution operator for control atom 1 as $U_{1,c1} = e^{i\gamma_1}|r\rangle_1\langle b| + e^{-i\gamma_1}|b\rangle_1\langle r| + |d\rangle_1\langle d|$ when $t \in (0, \frac{t_f}{2}]$ and for control atom 2 as $U_{1,c2} = e^{i\gamma_1}|r\rangle_2\langle b| + e^{-i\gamma_1}|b\rangle_2\langle r| + |d\rangle_2\langle d|$ when $t \in (\frac{t_f}{2}, t_f]$.

For all control atoms, setting $\alpha = 0$, and then $|b\rangle \equiv e^{i(\pi-\Phi)}|1\rangle$, $|d\rangle \equiv e^{i(\pi+\Phi)}|0\rangle$. And the evolution operators are simplified as $U'_{1,c1} = e^{i\gamma'_1}|r\rangle_1\langle 1| + e^{-i\gamma'_1}|1\rangle_1\langle r| + |0\rangle_1\langle 0|$ when $t \in (0, \frac{t_f}{2}]$ and for control atom 2 as $U'_{1,c2} = e^{i\gamma'_1}|r\rangle_2\langle 1| + e^{-i\gamma'_1}|1\rangle_2\langle r| + |0\rangle_2\langle 0|$ when $t \in (\frac{t_f}{2}, t_f]$, in which $\gamma'_1 = \gamma_1 + \Phi - \pi$ [see step (i) in Fig. 3].

Step (ii): Similarly to step (ii) in Sec. II A, if the parameters Ω and Φ_1 in Hamiltonian (13) are the same as Ω_0 and Φ_0 in Eq. (1), which are determined by Eq. (9), then the evolution operator would be $U_{2,T} = e^{i\gamma}|b\rangle_T\langle b| + e^{-i\gamma}|r\rangle_T\langle r| + |d\rangle_T\langle d|$ when $t \in (t_f, 2t_f]$ [see step (ii) in Fig. 3].

Step (iii): Similarly to step (iii) in Sec. II A, if the parameters Ω and Φ in Hamiltonian (13) are the same as Ω_0 and Φ_0 in Eq. (1), which are determined by Eqs. (10) and (11), then the evolution operator for control atoms 1 and 2 is $U_{3,c1} = e^{i\gamma_3}|b\rangle_1\langle r| + e^{-i\gamma_3}|r\rangle_1\langle b| + |d\rangle_1\langle d|$, $U_{3,c2} = e^{i\gamma_3}|b\rangle_2\langle r| + e^{-i\gamma_3}|r\rangle_2\langle b| + |d\rangle_2\langle d|$, respectively.

For all control atoms, setting $\alpha = 0$, the evolution operator in this step is simplified to $U_{3,c1} = e^{i\gamma'_3}|1\rangle_1\langle r| + e^{-i\gamma'_3}|r\rangle_1\langle 1| + |0\rangle_1\langle 0|$, $U_{3,c2} = e^{i\gamma'_3}|1\rangle_2\langle r| + e^{-i\gamma'_3}|r\rangle_2\langle 1| + |0\rangle_2\langle 0|$, respectively, in which $\gamma'_3 = \gamma_3 + \pi - \Phi$.

Combining steps (i) with (iii), the evolution operator for control atoms 1 and 2 is $U_{c1} = e^{i(\gamma_1+\gamma_3)}|1\rangle_1\langle 1| + e^{-i(\gamma_1+\gamma_3)}|r\rangle_1\langle r| + |0\rangle_1\langle 0|$ and $U_{c2} = e^{i(\gamma_1+\gamma_3)}|1\rangle_2\langle 1| + e^{-i(\gamma_1+\gamma_3)}|r\rangle_2\langle r| + |0\rangle_2\langle 0|$. $\gamma_1 + \gamma_3 = \gamma'$ and we set $\gamma' = 0$ for the C_2U gate [see step (iii) in Fig. 3]. After the above three steps, the gate $e^{i\gamma}|00b\rangle\langle 00b| + |00d\rangle\langle 00d| + |010\rangle\langle 010| + |100\rangle\langle 100| + |110\rangle\langle 110| + |011\rangle\langle 011| + |101\rangle\langle 101| + |111\rangle\langle 111|$ can be accomplished, which means C_kU ($k = 2$) is constructed if one reexpands the states $|b\rangle$ and $|d\rangle$ into the computational basis $|0\rangle$ and $|1\rangle$ [38,39].

C. The implementation of C_kU gate

The C_2U gate of the above scheme can be easily extended to the C_kU gate with the similar three steps. All the control and target atoms contain three levels of $|0\rangle$, $|1\rangle$, $|r\rangle$, as shown in Fig 1(b). As shown in Fig. 4, the first step is sequentially driving the control atoms one by one (note that α is still set as zero for all control atoms). The first control qubit in the $|1\rangle$ state will be excited to the $|r\rangle$ state, which means the remaining control atoms in the $|1\rangle$ state will no longer be excited due to the blockade effect. Meanwhile, the $|0\rangle$ state is decoupled in the whole process of the first step because α is set to zero. If there is no atom excited after the first step, the second step is the cyclic evolution of the target atom. Otherwise, if any of the control atoms are excited, there is no evolution of the target atom. The third step is the reverse process of the first step. The Hamiltonian of each atom can be written as

$$H_N = \Omega e^{i\Phi_1}|b\rangle_m\langle r| + \text{H.c.}\ (m = 1, 2, \cdots k, T), \tag{14}$$

where the definition of $|b\rangle$ is the same as that in Sec. II B. Considering Eq. (14) and the atom interaction H_I mentioned

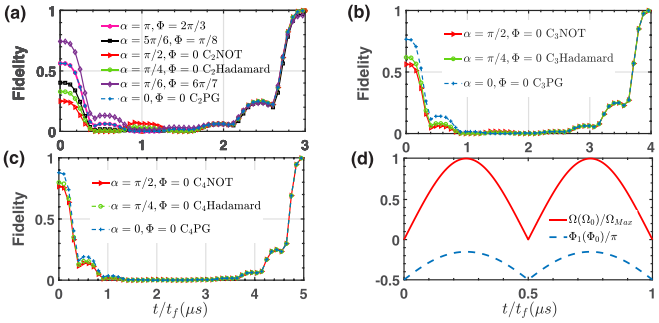

FIG. 5. (a) The fidelity of the C_2PG, C_2NOT, and C_2Hadamard gates; decay rate is $\Gamma = 1$ KHz. (b) The C_3PG, C_3NOT, and C_3Hadamard gate fidelity of the three-level case with $\Gamma = 1$ KHz. (c) The C_4PG, C_4NOT, and C_4Hadamard gate fidelity with $\Gamma = 1$ KHz. For (a)–(c), γ is set as π. (d) The pulse parameters corresponding to Eq. (1) and Eq. (14) during evolution and $\Phi_1(\Phi_0)$ for the target atom of C_kPG.

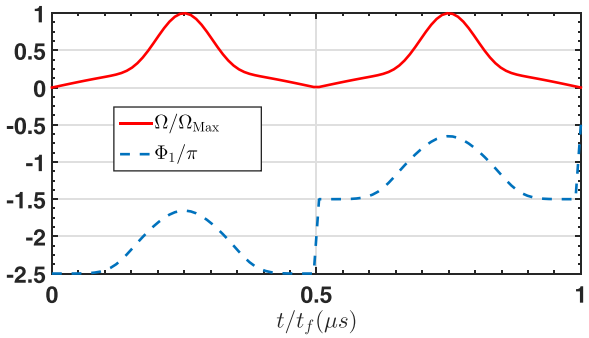

FIG. 6. Pulse and phase of ZSS-optimal scheme in Sec. II E.

above, with the condition $V_{ij} \gg \Omega$, the N-qubit C_kU gate

$$e^{i\gamma}|\underbrace{0\cdots0}_{k}b\rangle\langle\underbrace{0\cdots0}_{k}b| + (\hat{I}_N - |\underbrace{0\cdots0}_{k}b\rangle\langle\underbrace{0\cdots0}_{k}b|) \quad (15)$$

would be constructed, where $N = k + 1$ stands for k control atoms and one target atom. Here, γ can be an arbitrarily geometric phase angle.

If we expand the states of the target atom $|b\rangle$ and $|d\rangle$ into the basis $|0\rangle$ and $|1\rangle$, the multiple-qubit universal quantum logic gate can be constructed. After using the master equation for simulation, the fidelity of the C_2U, C_3U, and C_4U (U = PG, NOT, Hadamard) gates is shown in Figs. 5(a)–5(c), respectively, which show the feasibility and scalability of the scheme.

D. Performance of multiple-qubit gates

The performance of the C_kU gate can be evaluated by the Lindblad master equation

$$\dot{\rho} = -i[H, \rho] + \sum_{m=1}^{k} \frac{\Gamma}{2}(2L_m\rho L_m^\dagger - L_m^\dagger L_m\rho - \rho L_m^\dagger L_m), \quad (16)$$

where H and ρ are the Hamiltonian and the density matrix of the system, respectively, and $L_m = |0\rangle_m\langle r| + |1\rangle_m\langle r|$ are the Lindblad operators. Here, we set the fidelity of the gate to $F = |\langle\Psi_{\rm ideal}|\Psi_t\rangle|^2$, where $|\Psi_{\rm ideal}\rangle$ denotes the ideal final state calculated by performing the ideal quantum logic gate on the initial state. $|\Psi_t\rangle$ denotes the practical state at time t calculated by numerically solving the master equation. The initial state of the C_kU gate is set to $-\sum_{\mu_1\cdots\mu_k,T=0,1}(-1)^{\lceil(\mu_1+\cdots+\mu_k+T)/(k+1)\rceil}|\mu_1\cdots\mu_k T\rangle$, where "$\lceil\ \rceil$" is a mathematical symbol for rounding up, i.e., $\lceil x_1\rceil = 0(-1 < x_1 \leqslant 0)$, $\lceil x_2\rceil = 1(0 < x_2 \leqslant 1)$. The decay rate is chosen as $\Gamma = 1$ kHz and the duration of evolution is $t_f \approx 51.6$ ns. As shown in Figs. 5(a)–5(c), one can get different gates by choosing different parameters; for example, if $\alpha = \pi/2$, $\Phi = 0$, we can obtain the C_kNOT gate, and the parameters of $\alpha = \pi/4$, $\Phi = 0$ and $\alpha = 0$, $\Phi = 0$ correspond to the C_kHadamard gate and C_kPG gate, respectively. As for the fidelity of the gates, the C_2PG, C_2NOT, and C_2Hadamard gates can, respectively, reach 0.99839, 0.99847, and 0.99842, and the C_3PG, C_3NOT, and C_3Hadamard gates can, respectively, reach 0.99831, 0.99826, and 0.99841. Significantly, when the control atoms are expanded to four, the fidelity decreases slightly, and the C_4PG, C_4NOT, and C_4Hadamard gates can, respectively, reach 0.9977, 0.9979, and 0.9978. The corresponding parameters of $\Omega(\Omega_0)$ and $\Phi_1(\Phi_0)$ are shown in Fig. 5(d) in which $\Omega_{\rm Max} = 2\pi \times 16$ MHz. The Rydberg-Rydberg interaction strength is set as $V = 2\pi \times 400$ MHz, and $V \gg \Omega_{\rm Max}$ guarantees the Rydberg blockade effect of the system.

E. Optimal control

In order to make our scheme more robust to systematic errors, we adopt the zero systematic-error sensitivity (ZSS)-optimal protocol to further eliminate the errors; in particular, we consider the existence of a random static system error [104]. To begin with, we assume $\Omega \to (1+\epsilon)\Omega$, where ϵ is a small influence representing a systematic error, and then the Hamiltonian given by Eq. (14) can be rewritten as

$$H_\epsilon = (1+\epsilon)\Omega e^{i\Phi_1}|b\rangle_m\langle r| + \text{H.c.} \quad (17)$$

Since the evolution path is symmetric, we take the evolution of stage $(0, \frac{t_f}{2})$ as an example to study. According to the perturbation theory, we can obtain

$$P = |\langle\Psi_{(tf/2)}|\Psi_{\epsilon(tf/2)}\rangle|^2 = 1 + O_1 + O_2 + \cdots, \quad (18)$$

where $|\Psi_\epsilon\rangle$ is the state with the static error, and O_n denotes the term of the perturbation at the nth order. Here we only consider second-order perturbations, i.e., $P_2 = 1 + O_1 + O_2 = 1 - \epsilon^2 q_s$. According to Eqs. (3), (4), and (13), we can obtain the expression of $q_s = |\int_0^{tf/2} dt e^{-2ig}\dot{\chi}\sin^2\chi|^2$, where q_s represents the sensitivity of the system error. In order to eliminate the system error, one can set $g(\chi) = \frac{n}{2}[2\chi - \sin(2\chi)]$, and q_s can be further reduced to $q_s = \frac{\sin(n\pi)^2}{4n^2}$. The zero systematic error is realized when n is a positive integer. In the numerical simulation, we uniformly set the maximum value of Ω as $\Omega_{\rm Max} = 2\pi \times 16$ MHz, which is the same as the nonoptimization scheme, and thus the improvement of the gate fidelity can only be attributed to optimal control.

In this article, we take the C_kNOT ($k = 2$) gate of the target atom of a three-level couple as an example. Then we set $\varphi = -4n\sin^3\chi/3$ and $\chi = \pi\sin^2(\frac{\pi t}{t_f})$. The optimized pulse parameters are shown in Fig. 6. Next, we need to find the optimal

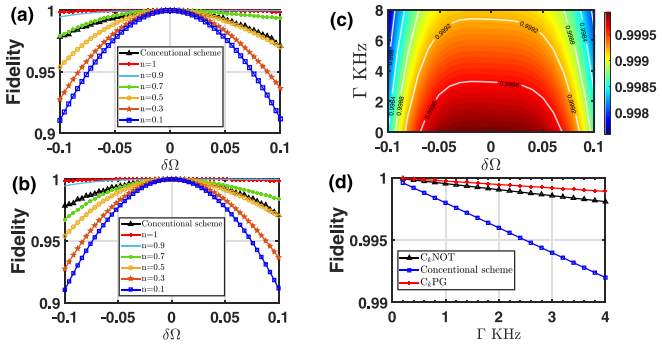

FIG. 7. The performance of the C_2NOT gate under the three-level case with optimization compared with the conventional scheme (Ω is a time-independent pulse scheme [98]). (a) The fidelity with different values n under the static error without decoherence. (b) The fidelity with different values n under the static error with $\Gamma = 1$ KHz. (c) Fidelity of gates at different decay rates and the static error with $n = 1$. (d) The fidelity of C_2NOT in two schemes (conventional scheme and our scheme) and C_2PG gate under different decoherence rates.

value of n under decoherence. As shown in Fig. 7, we simulate the C_2NOT gate fidelity under the systematic error from -0.1 to 0.1 and change n from 0 to 1. In this way, we find that $n = 1$ is always an optimal value, whether or not decoherence exists. Under the same parameters $\Omega_{\text{Max}} = 2\pi \times 16$ MHz and $V = 2\pi \times 400$ MHz, we compare the fidelity and robustness of the C_2NOT gates between our scheme and the conventional pulses scheme in Ref. [98]. In Fig. 7(b), when $\Gamma = 1$ KHz, the laser parameter $\delta\Omega$ fluctuates in the range of -0.1 to 0.1. Figure 7(d) shows the variation of the fidelity for the C_kU and conventional C_2NOT gate under the different spontaneous emission decay rates, where the decay rate Γ is modulated from 0.2 to 4 KHz. In total, the fidelity under the parameter fluctuation demonstrates that our scheme is indeed robust, and the speed of the gate is also certain, according to the adoption of STA.

III. EXPERIMENTAL CONSIDERATIONS

A. Realization of the pulse

We suppose d as the distance of two identical Rydberg atoms which are trapped in optical tweezers, and the strength of the van der Waals interaction (vdWI) is $V = C_6/d^6$ [105]. Furthermore, we apply an amplitude-modulation field of the Rabi frequency, $\Omega = \Omega_{(t)}e^{i\Phi_{(t)}}$, to atoms to drive the ground state $|1\rangle$ or $|b\rangle$ to Rydberg state $|r\rangle$. Such an amplitude-modulation field could be fulfilled by an acousto-optic modulator (AOM) with the assistance of the arbitrary waveform generator [22], and the laser phase could be modulated by a spatial light modulator (SLM). One of the most commonly used spatial light modulators is the liquid crystal spatial light modulator (LC-SLM) [106,107].

B. Rydberg atomic level structure

We choose $|r\rangle \equiv |83S, J = 1/2, m_J = 1/2\rangle$ for a rubidium atom as the Rydberg state and the vdWI coefficient of this atom is $C_6 = 9.7 \times 10^3$ GHz μm^6 [108]. According to Refs. [24,109], the Rydberg state lifetime is about $\tau = 696.35$ μs at a temperature of 0 K, and the correspond decay rate is $\Gamma = 1/\tau = 0.0014$ MHz. Two stable ground states can be chosen as $|0\rangle \equiv |5S_{1/2}, F = 1, m_F = 0\rangle$ and $|1\rangle \equiv |5S_{1/2}, F = 2, m_F = 0\rangle$, respectively [110]. The excitations from the two ground states to Rydberg states are realized by a two-photon process via the intermediate state $|5P_{1/2}\rangle$ or $|5P_{3/2}\rangle$. The Rabi frequency can be obtained as $\Omega = 2\pi \times 10$ MHz by setting the detuning of the two-photon process and the coupling strength between the ground (Rydberg) state and the intermediate state. The distance between the two identical Rydberg atoms is $d = 5.5$ μm, and the Rydberg interaction intensity is $V = 2\pi \times 350$ MHz in this way. Considering the above experimental parameters with the nonoptimized case, the fidelity of the C_2NOT, C_2Hadamard, and C_2PG gates constructed by our scheme is 0.9981, 0.9981, and 0.9982, respectively. If optimized again, the fidelity of the C_2U gate can still reach more than 0.999, which still has good fidelity whether optimal or not. The C_3PG, C_3NOT, and C_3Hadamard gates can, respectively, reach 0.9970, 0.9971, and 0.9971, and when the control atoms are expanded to four, the fidelity decreases slightly, and the C_4PG, C_4NOT, and C_4Hadamard gates can, respectively, reach 0.99603, 0.99605, and 0.99603 under the above experimental parameters.

C. Error analysis

Inspired by the results in Ref. [98], here we give the analytical result of the error by taking into account some internal errors, including spontaneous emission from the Rydberg state and finite blockade shift errors. The total error of the C_kNOT error can be given as [98]

$$\varepsilon_{\text{opt}} \simeq \frac{3\pi^{2/3}}{2^{1/3}}\frac{k}{(V\tau)^{2/3}} + \frac{\pi^{4/3}}{2^{8/3}}\frac{k^2}{(V\tau)^{4/3}}. \tag{19}$$

Here, k is the control qubit number and V is the strength of the vdWI. It should be noted that the establishment of Eq. (19) needs to meet certain conditions, including $V \gg \Omega \gg 1/\tau$ and $V\tau \gg k$. All these conditions are satisfied in our scheme. Then we obtain the maximum approximate error estimate of 0.0039 by taking $k = 2$ and $V = C_6/d^6 = 2\pi \times 350$ MHz as examples. In our scheme, the Rabi frequency Ω is time dependent, but we use the value of Ω_{Max} when we calculate the maximum error. Considering the maximum approximate error and spontaneous emission rate, the fidelity of the unoptimized C_2U gate fidelity is 0.9942.

D. Possible experimental configurations

With the development of quantum technology of Rydberg atoms trapped in optical lattices or tweezer arrays, a number of practical configurations of atomic arrays can be used to realize the proposed multiple-qubit gates, which satisfy the Rydberg blockade condition. Concretely, the one-dimensional [29,111,112] and two-dimensional [113,114] atomic array structures as well as the spherical structure [115] can be considered for the experimental realization of the desired gate.

IV. CONCLUSION

In general, we use the Rydberg blockade effect combined with shortcut to adiabaticity of inverse engineering and geometric quantum operations to construct a C_kU gate with high fidelity and high speed. In addition, our scheme is further optimized by the ZSS method and compared with the conventional scheme with the same parameters; the results show that our scheme is more robust and faster than the conventional and nonadiabatic scheme, respectively. Finally, the experimental implementation of the scheme is analyzed and the numerical simulation is carried out to further verify the feasibility of the scheme with the high fidelity and robustness.

ACKNOWLEDGMENTS

This work is supported by the National Natural Science Foundation of China (Grants No. 11804308, No. 11804375, and No. 12074346) and Natural Science Foundation of Henan Province (Grant No. 202300410481).

[1] M. Saffman, T. G. Walker, and K. Mølmer, Rev. Mod. Phys. **82**, 2313 (2010).
[2] D. Jaksch, J. I. Cirac, P. Zoller, S. L. Rolston, R. Côté, and M. D. Lukin, Phys. Rev. Lett. **85**, 2208 (2000).
[3] M. D. Lukin, M. Fleischhauer, R. Cote, L. M. Duan, D. Jaksch, J. I. Cirac, and P. Zoller, Phys. Rev. Lett. **87**, 037901 (2001).
[4] T. F. Gallagher, *Rydberg Atoms*, Vol. 3 (Cambridge University Press, Cambridge, 2005).
[5] D. Petrosyan, F. Motzoi, M. Saffman, and K. Mølmer, Phys. Rev. A **96**, 042306 (2017).
[6] H. Levine, A. Keesling, A. Omran, H. Bernien, S. Schwartz, A. S. Zibrov, M. Endres, M. Greiner, V. Vuletić, and M. D. Lukin, Phys. Rev. Lett. **121**, 123603 (2018).
[7] S.-L. Su, E. Liang, S. Zhang, J.-J. Wen, L.-L. Sun, Z. Jin, and A.-D. Zhu, Phys. Rev. A **93**, 012306 (2016).
[8] D. Comparat and P. Pillet, J. Opt. Soc. Am. B. **27**, A208 (2010).
[9] L. Béguin, A. Vernier, R. Chicireanu, T. Lahaye, and A. Browaeys, Phys. Rev. Lett. **110**, 263201 (2013).
[10] M. Saffman, J. Phys. B-At. Mol. Opt. **49**, 202001 (2016).
[11] T. Wilk, A. Gaëtan, C. Evellin, J. Wolters, Y. Miroshnychenko, P. Grangier, and A. Browaeys, Phys. Rev. Lett. **104**, 010502 (2010).
[12] E. Brion, A. S. Mouritzen, and K. Mølmer, Phys. Rev. A **76**, 022334 (2007).
[13] A. Gaëtan, Y. Miroshnychenko, T. Wilk, A. Chotia, M. Viteau, D. Comparat, P. Pillet, A. Browaeys, and P. Grangier, Nat. Phys. **5**, 115 (2009).
[14] M. Saffman, I. I. Beterov, A. Dalal, E. J. Páez, and B. C. Sanders, Phys. Rev. A **101**, 062309 (2020).
[15] X.-F. Shi, Phys. Rev. Appl. **7**, 064017 (2017).
[16] A. Mitra, M. J. Martin, G. W. Biedermann, A. M. Marino, P. M. Poggi, and I. H. Deutsch, Phys. Rev. A **101**, 030301(R) (2020).
[17] I. I. Beterov, M. Saffman, E. A. Yakshina, V. P. Zhukov, D. B. Tretyakov, V. M. Entin, I. I. Ryabtsev, C. W. Mansell, C. MacCormick, S. Bergamini, and M. P. Fedoruk, Phys. Rev. A **88**, 010303(R) (2013).
[18] D. D. Bhaktavatsala Rao and K. Mølmer, Phys. Rev. A **89**, 030301(R) (2014).
[19] I. I. Beterov, I. N. Ashkarin, E. A. Yakshina, D. B. Tretyakov, V. M. Entin, I. I. Ryabtsev, P. Cheinet, P. Pillet, and M. Saffman, Phys. Rev. A **98**, 042704 (2018).
[20] S.-L. Su, F.-Q. Guo, L. Tian, X.-Y. Zhu, L.-L. Yan, E.-J. Liang, and M. Feng, Phys. Rev. A **101**, 012347 (2020).
[21] X.-F. Shi, Phys. Rev. Appl. **14**, 054058 (2020).
[22] J.-L. Wu, S.-L. Su, Y. Wang, J. Song, Y. Xia, and Y.-Y. Jiang, Opt. Lett. **45**, 1200 (2020).
[23] F. Robicheaux, T. M. Graham, and M. Saffman, Phys. Rev. A **103**, 022424 (2021).
[24] L. Isenhower, E. Urban, X. L. Zhang, A. T. Gill, T. Henage, T. A. Johnson, T. G. Walker, and M. Saffman, Phys. Rev. Lett. **104**, 010503 (2010).
[25] K. M. Maller, M. T. Lichtman, T. Xia, Y. Sun, M. J. Piotrowicz, A. W. Carr, L. Isenhower, and M. Saffman, Phys. Rev. A **92**, 022336 (2015).
[26] Y. Zeng, P. Xu, X. He, Y. Liu, M. Liu, J. Wang, D. J. Papoular, G. V. Shlyapnikov, and M. Zhan, Phys. Rev. Lett. **119**, 160502 (2017).
[27] C. J. Picken, R. Legaie, K. McDonnell, and J. D. Pritchard, Quantum Sci. Technol. **4**, 015011 (2018).
[28] I. S. Madjarov, J. P. Covey, A. L. Shaw, J. Choi, A. Kale, A. Cooper, H. Pichler, V. Schkolnik, J. R. Williams, and M. Endres, Nat. Phys. **16**, 857 (2020).
[29] H. Levine, A. Keesling, G. Semeghini, A. Omran, T. T. Wang, S. Ebadi, H. Bernien, M. Greiner, V. Vuletić, H. Pichler, and M. D. Lukin, Phys. Rev. Lett. **123**, 170503 (2019).
[30] Y. Aharonov and J. Anandan, Phys. Rev. Lett. **58**, 1593 (1987).
[31] F. Wilczek and A. Zee, Phys. Rev. Lett. **52**, 2111 (1984).
[32] P. Zanardi and M. Rasetti, Phys. Lett. A **264**, 94 (1999).
[33] V. V. Albert, C. Shu, S. Krastanov, C. Shen, R.-B. Liu, Z.-B. Yang, R. J. Schoelkopf, M. Mirrahimi, M. H. Devoret, and L. Jiang, Phys. Rev. Lett. **116**, 140502 (2016).
[34] M. V. Berry, Proc. R. Soc. Lond. **392**, 45 (1984).
[35] S.-L. Zhu and Z. D. Wang, Phys. Rev. Lett. **89**, 097902 (2002).
[36] Wang Xiang-Bin and M. Keiji, Phys. Rev. Lett. **87**, 097901 (2001).
[37] L.-M. Duan, J. I. Cirac, and P. Zoller, Science **292**, 1695 (2001).
[38] E. Sjöqvist, D. M. Tong, L. M. Andersson, B. Hessmo, M. Johansson, and K. Singh, New J. Phys. **14**, 103035 (2012).
[39] G. F. Xu, J. Zhang, D. M. Tong, E. Sjöqvist, and L. C. Kwek, Phys. Rev. Lett. **109**, 170501 (2012).
[40] M. Johansson, E. Sjöqvist, L. M. Andersson, M. Ericsson, B. Hessmo, K. Singh, and D. M. Tong, Phys. Rev. A **86**, 062322 (2012).
[41] A. A. Abdumalikov Jr, J. M. Fink, K. Juliusson, M. Pechal, S. Berger, A. Wallraff, and S. Filipp, Nature (London) **496**, 482 (2013).
[42] J. Spiegelberg and E. Sjöqvist, Phys. Rev. A **88**, 054301 (2013).
[43] V. A. Mousolou, C. M. Canali, and E. Sjöqvist, New J. Phys. **16**, 013029 (2014).

[44] S. Arroyo-Camejo, A. Lazariev, S. W. Hell, and G. Balasubramanian, Nat. Commun. **5**, 4870 (2014).

[45] G. Xu and G. Long, Sci. Rep. **4**, 6814 (2014).

[46] J. Zhou, W.-C. Yu, Y.-M. Gao, and Z.-Y. Xue, Opt. Express **23**, 14027 (2015).

[47] Z.-Y. Xue, J. Zhou, and Z. D. Wang, Phys. Rev. A **92**, 022320 (2015).

[48] Y. Wang, J. Zhang, C. Wu, J. Q. You, and G. Romero, Phys. Rev. A **94**, 012328 (2016).

[49] P. Z. Zhao, G. F. Xu, Q. M. Ding, E. Sjöqvist, and D. M. Tong, Phys. Rev. A **95**, 062310 (2017).

[50] Z.-Y. Xue, F.-L. Gu, Z.-P. Hong, Z.-H. Yang, D.-W. Zhang, Y. Hu, and J. Q. You, Phys. Rev. Appl. **7**, 054022 (2017).

[51] Y. Sekiguchi, N. Niikura, R. Kuroiwa, H. Kano, and H. Kosaka, Nat. Photon. **11**, 309 (2017).

[52] Z.-P. Hong, B.-J. Liu, J.-Q. Cai, X.-D. Zhang, Y. Hu, Z. D. Wang, and Z.-Y. Xue, Phys. Rev. A **97**, 022332 (2018).

[53] G. T. Genov, D. Schraft, N. V. Vitanov, and T. Halfmann, Phys. Rev. Lett. **118**, 133202 (2017).

[54] P. Z. Zhao, X. Wu, and D. M. Tong, Phys. Rev. A **103**, 012205 (2021).

[55] G. F. Xu, C. L. Liu, P. Z. Zhao, and D. M. Tong, Phys. Rev. A **92**, 052302 (2015).

[56] B. B. Zhou, P. C. Jerger, V. O. Shkolnikov, F. J. Heremans, G. Burkard, and D. D. Awschalom, Phys. Rev. Lett. **119**, 140503 (2017).

[57] G. F. Xu, D. M. Tong, and E. Sjöqvist, Phys. Rev. A **98**, 052315 (2018).

[58] B.-J. Liu, X.-K. Song, Z.-Y. Xue, X. Wang, and M.-H. Yung, Phys. Rev. Lett. **123**, 100501 (2019).

[59] E. Sjöqvist, Phys. Lett. A **380**, 65 (2016).

[60] E. Herterich and E. Sjöqvist, Phys. Rev. A **94**, 052310 (2016).

[61] Y. Xu, W. Cai, Y. Ma, X. Mu, L. Hu, T. Chen, H. Wang, Y. P. Song, Z.-Y. Xue, Z.-q. Yin, and L. Sun, Phys. Rev. Lett. **121**, 110501 (2018).

[62] Z. Zhu, T. Chen, X. Yang, J. Bian, Z.-Y. Xue, and X. Peng, Phys. Rev. Appl. **12**, 024024 (2019).

[63] X.-T. Yu, Q. Zhang, Y. Ban, and X. Chen, Phys. Rev. A **97**, 062317 (2018).

[64] T. Yan, B.-J. Liu, K. Xu, C. Song, S. Liu, Z. Zhang, H. Deng, Z. Yan, H. Rong, K. Huang, M.-H. Yung, Y. Chen, and D. Yu, Phys. Rev. Lett. **122**, 080501 (2019).

[65] T. Wang, Z. Zhang, L. Xiang, Z. Jia, P. Duan, W. Cai, Z. Gong, Z. Zong, M. Wu, J. Wu, L. Sun, Y. Yin, and G. Guo, New J. Phys. **20**, 065003 (2018).

[66] F. Kleißler, A. Lazariev, and S. Arroyo-Camejo, NPJ Quantum Inf. **4**, 49 (2018).

[67] J. A. Jones, V. Vedral, A. Ekert, and G. Castagnoli, Nature (London) **403**, 869 (2000).

[68] G. Feng, G. Xu, and G. Long, Phys. Rev. Lett. **110**, 190501 (2013).

[69] N. V. Vitanov, A. A. Rangelov, B. W. Shore, and K. Bergmann, Rev. Mod. Phys. **89**, 015006 (2017).

[70] N. V. Vitanov, K.-A. Suominen, and B. W. Shore, J. Phys. B-At. Mol. Opt. **32**, 4535 (1999).

[71] J. R. Kuklinski, U. Gaubatz, F. T. Hioe, and K. Bergmann, Phys. Rev. A **40**, 6741 (1989); N. Vitanov and S. Stenholm, Opt. Commun. **127**, 215 (1996); G. Grigoryan and Y. Pashayan, *ibid.* **198**, 107 (2001).

[72] D. Møller, L. B. Madsen, and K. Mølmer, Phys. Rev. A **75**, 062302 (2007); Phys. Rev. Lett. **100**, 170504 (2008).

[73] A. del Campo and K. Kim, New J. Phys. **21**, 050201 (2019).

[74] D. Guéry-Odelin, A. Ruschhaupt, A. Kiely, E. Torrontegui, S. Martínez-Garaot, and J. G. Muga, Rev. Mod. Phys. **91**, 045001 (2019).

[75] X. Chen, A. Ruschhaupt, S. Schmidt, A. del Campo, D. Guéry-Odelin, and J. G. Muga, Phys. Rev. Lett. **104**, 063002 (2010).

[76] X. Chen, I. Lizuain, A. Ruschhaupt, D. Guéry-Odelin, and J. G. Muga, Phys. Rev. Lett. **105**, 123003 (2010).

[77] Y.-H. Kang, Z.-C. Shi, Y. Xia, and J. Song, Adv. Quantum Technol. **3**, 2000113 (2020).

[78] D. Ran, B. Zhang, Y.-H. Chen, Z.-C. Shi, Y. Xia, R. Ianconescu, J. Scheuer, and A. Gover, Opt. Lett. **45**, 3597 (2020).

[79] X. Yang, R. Liu, J. Li, and X. Peng, Phys. Rev. A **102**, 012614 (2020).

[80] S. Deffner, C. Jarzynski, and A. del Campo, Phys. Rev. X **4**, 021013 (2014).

[81] Y.-H. Kang, Y.-H. Chen, Z.-C. Shi, B.-H. Huang, J. Song, and Y. Xia, Phys. Rev. A **97**, 042336 (2018).

[82] J. Zhang, T. H. Kyaw, D. M. Tong, E. Sjöqvist, and L.-C. Kwek, Sci. Rep. **5**, 18414 (2015).

[83] D. Stefanatos and E. Paspalakis, Phys. Rev. A **99**, 022327 (2019).

[84] H. R. Lewis and W. B. Riesenfeld, J. Math. Phys. **10**, 1458 (1969).

[85] Y.-H. Kang, Y.-H. Chen, Q.-C. Wu, B.-H. Huang, Y. Xia, and J. Song, Sci. Rep. **6**, 30151 (2016).

[86] R.-Y. Yan and Z.-B. Feng, Quantum Sci. Technol. **5**, 045001 (2020).

[87] X. Da and Z.-C. Shi, Ann. Phys. **532**, 2000093 (2020).

[88] Y. Wang, Y. Ding, J. Wang, and X. Chen, Entropy **22**, 1175 (2020).

[89] S. Liu, D. Ran, Y.-H. Kang, Z.-C. Shi, J. Song, and Y. Xia, Ann. Phys. **532**, 2000002 (2020).

[90] I. Lizuain, A. Tobalina, A. Rodriguez-Prieto, and J. G. Muga, Entropy **22**, 350 (2020).

[91] R.-H. Zheng, Y.-H. Kang, S.-L. Su, J. Song, and Y. Xia, Phys. Rev. A **102**, 012609 (2020).

[92] N. N. Hegade, K. Paul, Y. Ding, M. Sanz, F. Albarrán-Arriagada, E. Solano, and X. Chen, Phys. Rev. Appl. **15**, 024038 (2021).

[93] E. Urban, T. A. Johnson, T. Henage, L. Isenhower, D. D. Yavuz, T. G. Walker, and M. Saffman, Nat. Phys. **5**, 110 (2009).

[94] A. Barenco, C. H. Bennett, R. Cleve, D. P. DiVincenzo, N. Margolus, P. Shor, T. Sleator, J. A. Smolin, and H. Weinfurter, Phys. Rev. A **52**, 3457 (1995).

[95] M. Saffman and K. Mølmer, Phys. Rev. Lett. **102**, 240502 (2009).

[96] S.-B. Zheng, Phys. Rev. A **87**, 042318 (2013).

[97] M. A. Nielsen and I. Chuang, Am. J. Phys. **70**, 558 (2002).

[98] L. Isenhower, M. Saffman, and K. Mølmer, Quantum Inf. Process. **10**, 755 (2011).

[99] S. L. Su, Chin. Phys. B **27**, 110304 (2018).

[100] E. Brion, K. Mølmer, and M. Saffman, Phys. Rev. Lett. **99**, 260501 (2007).

[101] S. L. Su, H. Z. Shen, E. Liang, and S. Zhang, Phys. Rev. A **98**, 032306 (2018).
[102] M. Khazali and K. Mølmer, Phys. Rev. X **10**, 021054 (2020).
[103] S. Li, T. Chen, and Z.-Y. Xue, Adv. Quantum Technol. **3**, 2000001 (2020).
[104] A. Ruschhaupt, X. Chen, D. Alonso, and J. G. Muga, New J. Phys **14**, 093040 (2012).
[105] J. T. Young, P. Bienias, R. Belyansky, A. M. Kaufman, and A. V. Gorshkov, arXiv:2006.02486 (2020).
[106] U. Efron, *Spatial Light Modulator Technology: Materials, Devices, and Applications*, Vol. 47 (CRC Press, Boca Raton, FL, 1994).
[107] X.-L. Wang, J. Ding, W.-J. Ni, C.-S. Guo, and H.-T. Wang, Opt. Lett. **32**, 3549 (2007).
[108] W. Li, D. Viscor, S. Hofferberth, and I. Lesanovsky, Phys. Rev. Lett. **112**, 243601 (2014).
[109] X.-Y. Zhu, Z. Jin, E. Liang, S. Zhang, and S.-L. Su, Ann. Phys. **532**, 2000059 (2020).
[110] X. L. Zhang, L. Isenhower, A. T. Gill, T. G. Walker, and M. Saffman, Phys. Rev. A **82**, 030306(R) (2010).
[111] A. Omran, H. Levine, A. Keesling, G. Semeghini, T. T. Wang, S. Ebadi, H. Bernien, A. S. Zibrov, H. Pichler, S. Choi *et al.*, Science **365**, 570 (2019).
[112] M. Ebert, M. Kwon, T. G. Walker, and M. Saffman, Phys. Rev. Lett. **115**, 093601 (2015).
[113] A. W. Glaetzle, R. M. W. van Bijnen, P. Zoller, and W. Lechner, Nat. Commun. **8**, 15813 (2017).
[114] T. M. Graham, M. Kwon, B. Grinkemeyer, Z. Marra, X. Jiang, M. T. Lichtman, Y. Sun, M. Ebert, and M. Saffman, Phys. Rev. Lett. **123**, 230501 (2019).
[115] D.-M. Yu, W.-P. Zhang, J.-M. Liu, S.-L. Su, and J. Qian, arXiv:2007.11938.